Supporting Information

NMR experiments for studies of dilute and condensed protein phases: Application to the phase-separating protein CAPRIN1

Leo E. Wong[1-3]‡, Tae Hun Kim[1-4]‡, D. Ranjith Muhandiram[1-3], Julie D. Forman-Kay[2,4] and Lewis E. Kay[1-4*]

[1]Department of Molecular Genetics, University of Toronto, Toronto, Ontario M5S 1A8, Canada

[2]Department of Biochemistry, University of Toronto, Toronto, Ontario M5S 1A8, Canada

[3]Department of Chemistry, University of Toronto, Toronto, Ontario M5S 1A8, Canada

[4]Hospital for Sick Children, Program in Molecular Medicine, 555 University Avenue, Toronto, Ontario M5G 1X8, Canada

‡These authors contributed equally.

*Corresponding author: kay@pound.med.utoronto.ca

Comparative study of haCONHA and HNCO datasets recorded under identical conditions

It is of interest to compare signal-to-noise values of $^{1}H^{\alpha}$- and $^{1}H^{N}$-detect spectra that record ^{15}N and ^{13}CO chemical shifts. We have examined datasets recorded on CAPRIN1 at pH 5.5, 25^{o}C where the effects of solvent hydrogen exchange on the quality of HNCO spectra are expected to be tolerable, in general, and at pH 7.4, 25^{o}C, where exchange is predicted to be pathologic. As HNCO datasets also include correlations from Gly residues, a compromise τ_2 delay was chosen for recording the haCONHA (2.3 ms, scheme of Figure 2A, using coherence selection that affords better water suppression) so that all residue-types are present in the spectra. Cross-peaks in the HNCO measured at pH 5.5 are of higher sensitivity, on average by a factor of 2.5-3 for correlations where magnetization does not originate on either of Ser or Gly (Figure S5A) and more for Ser or Gly (see legend to Figure S5). The variation in relative sensitivity on a per-residue basis that is observed in Figure S5 reflects, in part, residue-specific relaxation that is more acute for the haCONHA as the pulse scheme is longer than for the HNCO as well as different contributions to each residue from solvent exchange in the HNCO dataset that can be non-negligible even at pH 5.5. It is worth emphasizing that an advantage of the haCONHA is that correlations involving Pro residues can also be obtained, unlike for the HNCO, although the HNCO remains the far superior experiment for applications to IDPs at lower pH. We have also performed a similar comparison on a dilute sample prepared at pH 7.4 and it is clear that the HNCO experiment is not viable, with the majority of expected cross peaks not observed. Notably, however, four HNCO correlations are of higher sensitivity than for the haCONHA. These originate from the C-terminal two residues and from a pair of Asp residues that are part of the IsoAsp-Gly linkages, as discussed in the main text. Recognizing the limitations of the HNCO scheme[1] that has been used here, we have designed an improved HNCO sequence for studies of protein systems with fast exchanging amides based on the CP-HISQC approach of Yuwen and Skrynnikov[2]. In this implementation solvent exchange can be exploited to increase the transfer of magnetization from $^{1}H^{N}$ to ^{15}N during an initial cross-polarization element. Indeed, the 'new' HNCO was,

on average, a factor of two more sensitive than the previous version, but S/N ratios ('new' HNCO *vs* haCONHA) for 2/3 of the correlations were still under 0.1.

Supporting Figures

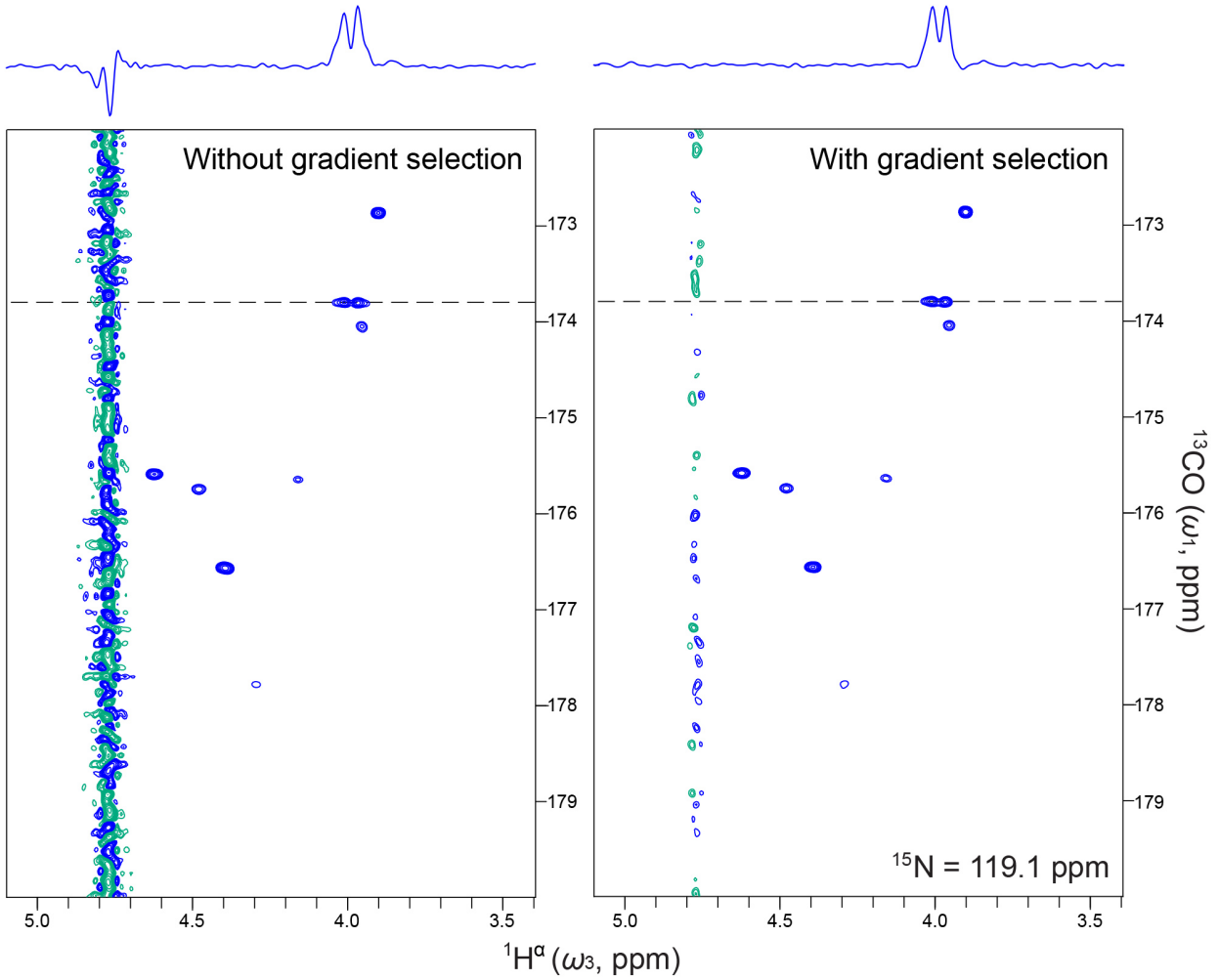

Figure S1. Comparison of water suppression levels obtained using haCONHA schemes of Figure 2C (left) and 2D (right). Separate 3D datasets were recorded on a dilute CAPRIN1 sample (25mM MES, pH 5.5) in a 5-mm tube at 25°C (98% H_2O, 2% D_2O) with τ_2 = 2.3 ms, using NUS, to give measurement times of 5 hours/dataset. A pair of planes are illustrated (^{15}N shift of 119.1 ppm), along with a horizontal trace at a ^{13}CO shift of 173.8 ppm (dashed line) that emphasizes the improved water suppression with scheme 2D.

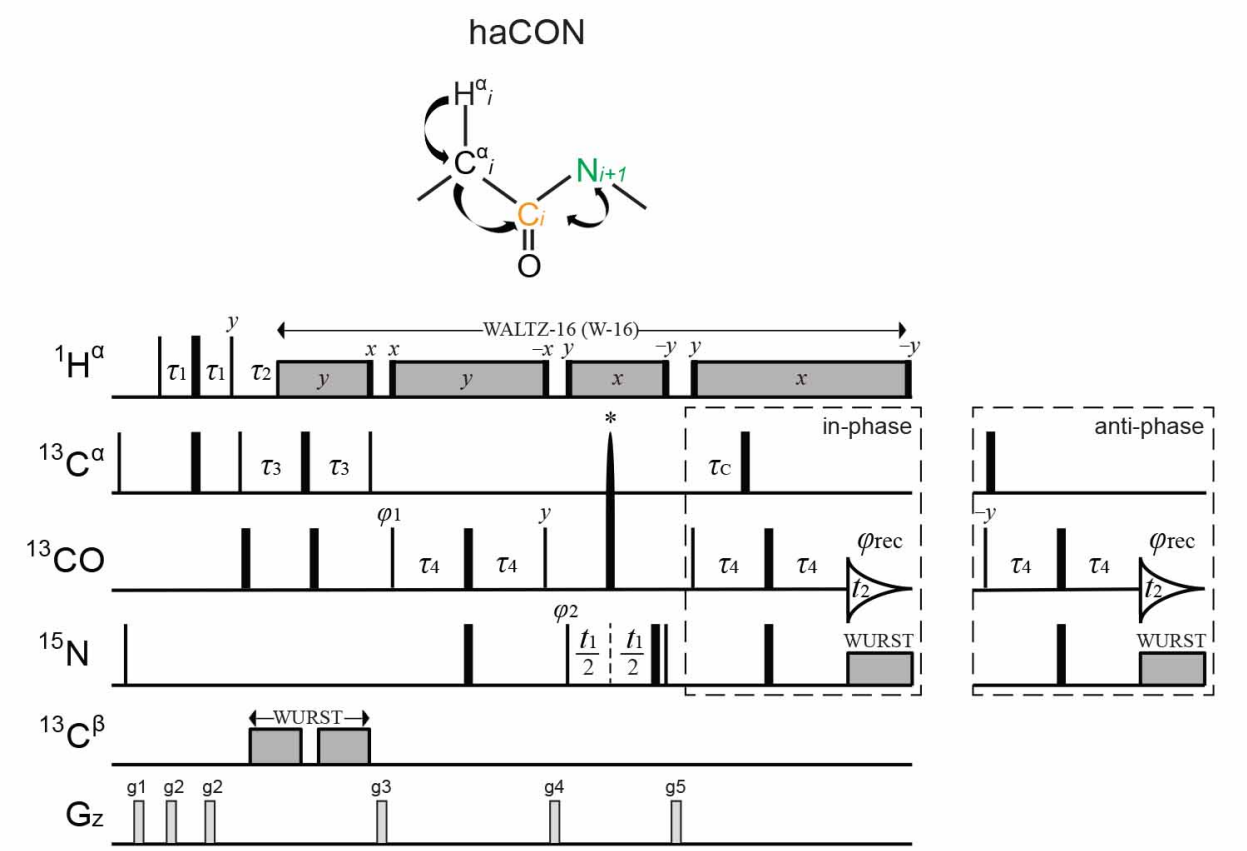

Figure S2. (A) Pulse sequence of the haCON for recording correlations of the form ($^{15}N_{i+1}$,$^{13}CO_i$). All 90° (180°) rectangular pulses are denoted by narrow (wide) bars and are applied along the x-axis unless otherwise indicated. ^{1}H, ^{13}C, and ^{15}N carriers are placed on water (~4.7 ppm), 58 ppm (until immediately before the ^{13}CO pulse of phase φ_1 when the carrier is jumped to 176 ppm for the remainder of the sequence), and 119 ppm, respectively. Composite pulse decoupling is denoted by grey boxes; in the event that decoupling is not along the x axis the phase is indicated inside the box. ^{1}H WALTZ-16 decoupling[3] as well as the flanking 90° pulses are applied with a field of ~6.25 kHz. $^{13}C^{\alpha}$ and ^{13}CO 90° and 180° rectangular pulses are applied with fields of $\Delta\Omega/\sqrt{15}$ and $\Delta\Omega/\sqrt{3}$, respectively, where $\Delta\Omega$ = 118 ppm[4]. A Bloch-Siegert compensation pulse (^{13}CO) is applied at the start of the τ_3 period[5]. The 400 μs ^{13}C adiabatic pulse denoted by an asterisk is applied with a field of ~11 kHz, 80 kHz sweep and centered at 117 ppm; its duration is compensated through the addition of a delay equal to the pulse width immediately after the ^{15}N 180° pulse that follows the t_1 period. Decoupling during t_2 is achieved using an ^{15}N WURST scheme with a sweep from 99 to 139 ppm[6]. The delays used are: τ_1 = 1.8 ms, τ_3 = 4.5 ms, τ_4 = 15 ms and τ_C = 4.76 ms (corresponding to $^{1}J_{CACO}$ of 52.5 Hz). The delay τ_2 is set to either 3.6 ms (for ^{13}CH) or 2.3 ms (both ^{13}CH and $^{13}CH_2$). $^{13}C^{\beta}$ WURST decoupling[7] is achieved using a waveform described in the legend to Figure 2. Removal of ^{13}CO-$^{13}C^{\alpha}$ couplings in F_2 results from combining in-phase and anti-phase spectra acquired in an interleaved manner[8,9]. The phase cycle used is: φ_1 = 2(x),2(−x); φ_2 = x,−x; and φ_{rec} = x,2(−x),x. Quadrature detection in t_1 is achieved by STATES-TPPI[10] of φ_2. Gradients are applied with the following durations (ms) and strengths (in % maximum): g1: (1.0, 14%), g2: (1.0, 17%), g3: (1.0, 27%),

g4: (1.0, 41%), g5: (1.0, 33%). The magnetization transfer pathway is depicted as a cartoon, where chemical shift encoding is color-coded as t_1 (green) and t_2 (gold).

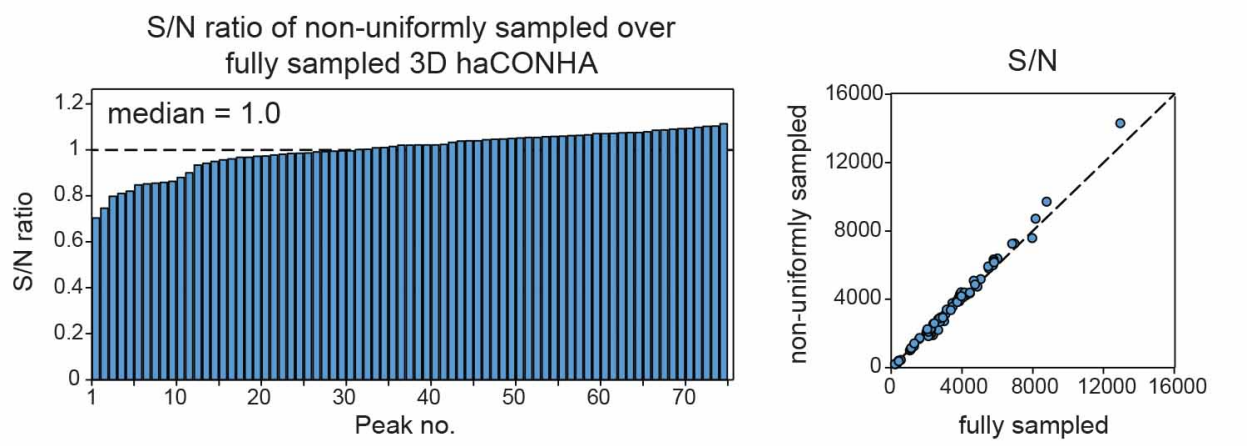

Figure S3. Comparison of S/N ratios of correlations in haCONHA spectra, acquired with uniform sampling and NUS (ratio = NUS/fully sampled). Data is sorted from lowest to highest S/N ratios. Datasets (pulse scheme of Figure 2A using gradient coherence transfer selection, panel D) were measured on a dilute CAPRIN1 sample (25 mM sodium phosphate, pH 7.4) at 30 °C with τ_2 = 3.6 ms (selection of AX spin systems), t_{1max} = 64 ms, t_{2max} = 55 ms, t_{3max} = 64 ms. The number of scans for the fully sampled and NUS (25.5 %) spectra are 2 and 8, respectively, for a total measurement time of 21 hours for both experiments.

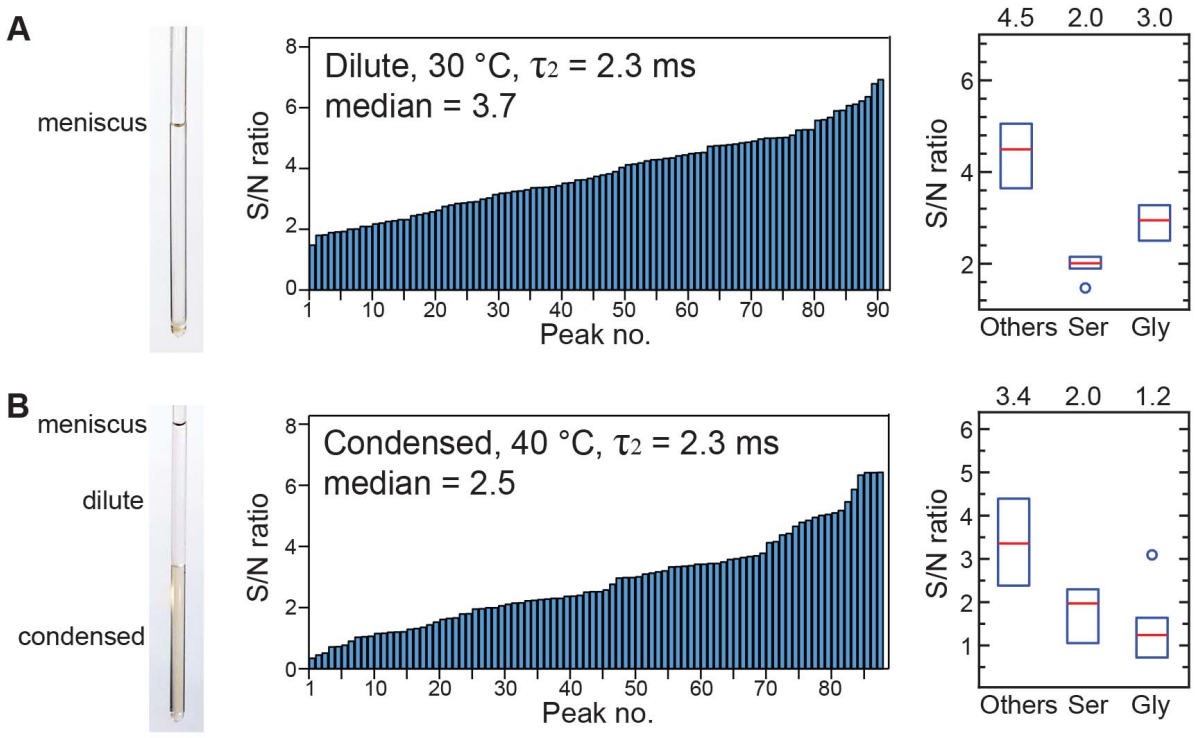

Figure S4. Comparison of S/N ratios (^{1}H detect/^{13}C detect) in spectra of haCONHA (3D; $^{1}H^{\alpha}$ detected using the sequence of Figure 2A with gradient coherence selection) and 2D haCON (2D; ^{13}C-detected) recorded on a sample of (A) dilute CAPRIN1 (25 mM NaPi, pH 7.4, 30^{o}C, 5 mm NMR tube) or (B) condensed CAPRIN1 (25 mM NaPi, pH 7.4, 100 mM NaCl, 40^{o}C, 3 mm NMR tube). Details are as in the legend to Figure 3 with the exception that τ_2=2.3 ms so that signals from all amino acids are observed. Identical net spectral acquisition times (21 hr) were used for all datasets, acquired with uniform sampling. To the right of each histogram is shown 'box plots', as in Figure 3, with the median highlighted in red and indicated above each box.

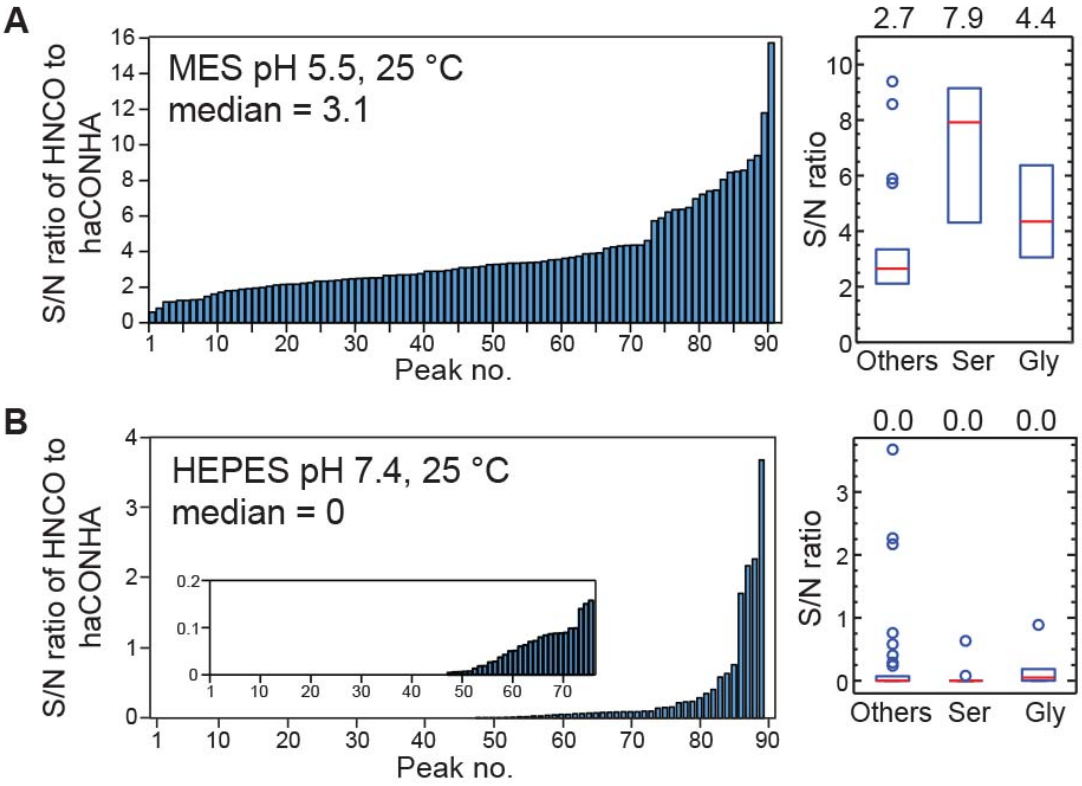

Figure S5. Comparison of signal-to-noise (S/N) ratios in HNCO (sensitivity enhanced pulse scheme with water flip-back[1]) and haCONHA (sequence of Figure 2A, with scheme D) 3D spectra. Datasets were recorded on dilute samples of either 25 mM MES, pH 5.5, 25°C (A) or 25 mM HEPES, pH 7.4, 25°C (B). All residues, including Gly, were selected in the haCONHA experiments by setting τ_2=2.3 ms in the scheme of Figure 2A. Additional experimental details are provided in Table S1. Residues were analyzed by first dividing them into 3 groups corresponding to "Others", Ser, and Gly, with the median S/N ratio for each group denoted by red lines and indicated numerically on top of each box; other details are as in Figure 3. Calculated S/N ratios, neglecting relaxation, are 2.1, 7.1 and 2.5 for 'Others', 'Ser', and 'Gly', respectively (see below). The lower calculated *vs* experimental value in the case of Gly likely reflects relaxation losses in the haCONHA during the intervals that include the defocusing and refocusing of $^{13}C^{\alpha}$ magnetization with respect to the attached ^{13}CO spin that are more significant for this residue than other amino acids for which only a single proton is attached to the C^{α} carbon. In addition, despite the fact that the $^{13}C^{\beta}$ decoupling waveform does not encompass the Gly $^{13}C^{\alpha}$ chemical shift region we have observed

that there is still an effect on $^{13}C^{\alpha}$ magnetization for this amino acid, leading to additional sensitivity losses. In (B), a value of 0 is assigned to peaks that could not be detected.

S/N ratios (HNCO/haCONHA) were calculated by neglecting relaxation during the delays in the pulse schemes as well as any losses in the HNCO due to solvent hydrogen exchange (low pH limit) using the following equations:

$$\text{“Others”: S/N} = \frac{\sqrt{2}}{\sin^2(\pi J_{HC}\tau_2)\frac{1+\sin(\pi J_{HC}\tau_2)}{2}}$$

$$\text{Ser: S/N} = \frac{\sqrt{2}}{\sin^2(\pi J_{HC}\tau_2)\frac{1+\sin(\pi J_{HC}\tau_2)}{2}\cos^2(2\pi J_{CC}\tau_3)}$$

$$\text{Gly: S/N} = \frac{\sqrt{2}}{\sin^2(2\pi J_{HC}\tau_2)\frac{\cos(\pi J_{HC}\tau_2)+\sin(\pi J_{HC}\tau_2)}{2}}$$

where J_{HC} is the one-bond $^{1}H^{\alpha}$-$^{13}C^{\alpha}$ scalar coupling (140 Hz) and the τ_i values are as in Figure 2A. In these expressions the factor of √2 in the numerator derives from the fact that the HNCO scheme is recorded in sensitivity-enhanced mode[11,12], the factors $\sin^2(\pi J_{HC}\tau_2)$ (“Others” or Ser; AX spin systems) and $\sin^2(2\pi J_{HC}\tau_2)$ (Gly; AX_2 spin system) account for the losses in the haCONHA from the compromise τ_2 delay used to refocus/defocus anti/in-phase $^{13}C^{\alpha}$ magnetization (2.3 ms). The $\cos^2(2\pi J_{CC}\tau_3)$ factor for Ser is due to the evolution of $^{13}C^{\alpha}$ magnetization from the one-bond $^{13}C^{\alpha}$-$^{13}C^{\beta}$ scalar coupling that is not decoupled, as the $^{13}C^{\beta}$ decoupling bandwidth does not extend to include the Ser $^{13}C^{\beta}$ chemical shift range (see text). Finally, the additional terms in the equations include further losses from the gradient selected element at the end of the scheme of Figure 2D, as described in the text. It should be noted that the expression for Gly S/N includes contributions from both H^{α} protons; both protons were included in evaluating the S/N experimentally.

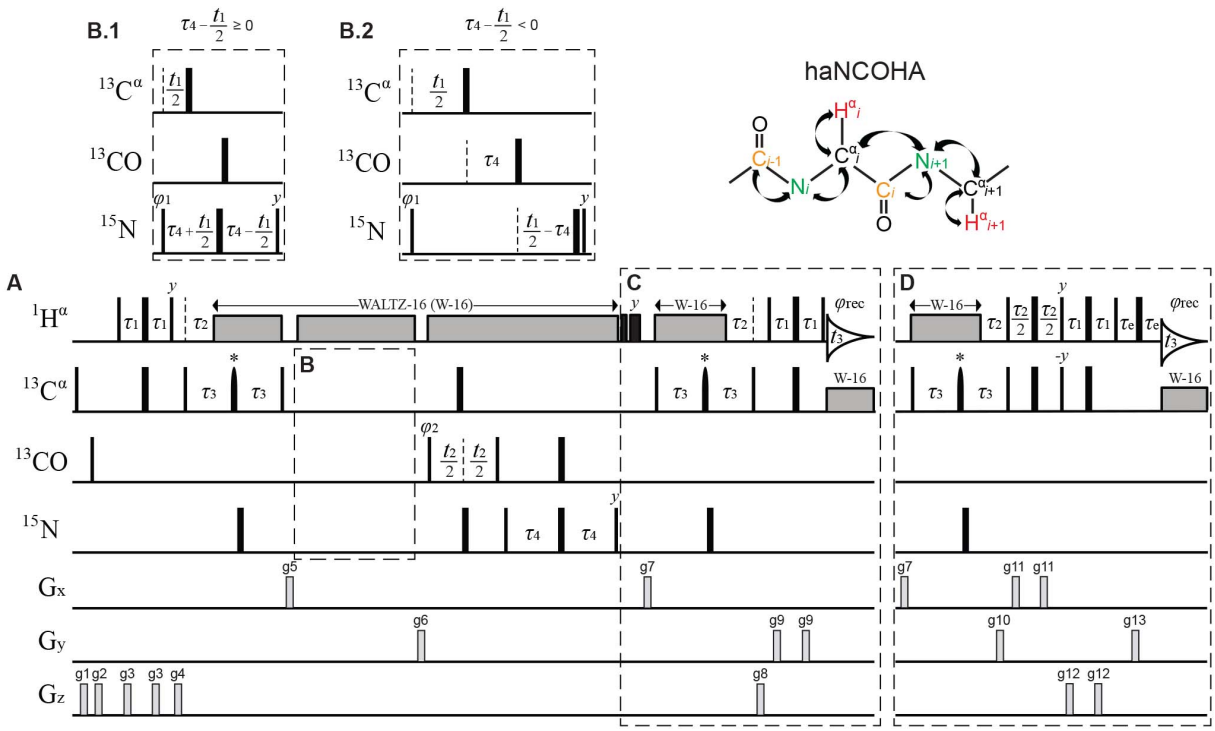

Figure S6. (A) haNCOHA pulse scheme providing correlations of the form ($^{15}N_{i+1}$,$^{13}CO_i$,$^{1}H^{\alpha}_i$) and ($^{15}N_i$,$^{13}CO_{i-1}$,$^{1}H^{\alpha}_i$). The magnetization transfer pathway is illustrated along with nuclei whose chemical shifts are encoded, color-coded as t_1 (green), t_2 (gold), and t_3 (red). Many of the details have been described in Figure 2 and are not repeated here. ^{1}H, ^{13}C, and ^{15}N carriers are placed on water (~4.7 ppm), 58 ppm (until immediately before the ^{13}CO pulse of phase φ_2 when the carrier is jumped to 176 ppm and then returned to 58 ppm after the ^{13}CO 90° pulse that completes the t_2 evolution period), and 119 ppm, respectively. The ^{13}C pulses denoted by asterisks have the REBURP shape[13], are applied with sufficient power to cover the complete aliphatic bandwidth (~15.7 kHz, 400 µs at 600 MHz) and are centered at 43 ppm. The delays are: τ_1 = 1.8 ms, τ_2 = 3.6 ms (^{13}CH) or 2.3 ms (^{13}CH + $^{13}CH_2$), τ_3 = 13.5 ms, τ_4 = 15 ms. A shared constant-time acquisition scheme[14,15] is used for recording ^{15}N (B.1 and B.2). Back-transfer of magnetization to $^{1}H^{\alpha}$ is achieved with either scheme (C) or (D), with the gradient selection approach of (D) recommended for water samples. The phase cycle is: $\varphi_1 = x,-x$; $\varphi_2 = 2(x),2(-x)$; and $\varphi_{rec} = x,2(-x),x$. Quadrature detection in t_1 and t_2 is achieved by STATES-TPPI[10] of φ_1 and φ_2, respectively. Gradients are applied with the following durations (ms) and strengths (in % maximum): g1: (0.5, 24%), g2: (1.0, 24%), g3: (0.256, 15%), g4: (1.0, 40%), g5: (1.25, 80%), g6: (0.8, 60%), g7: (1.5, 80%), g8: (0.3, −20%), g9: (0.4, −20%), g10: (1.024, 90%), g11: (0.4, 40%), g12: (0.3, 15%), g13: (0.256, 90.3%).

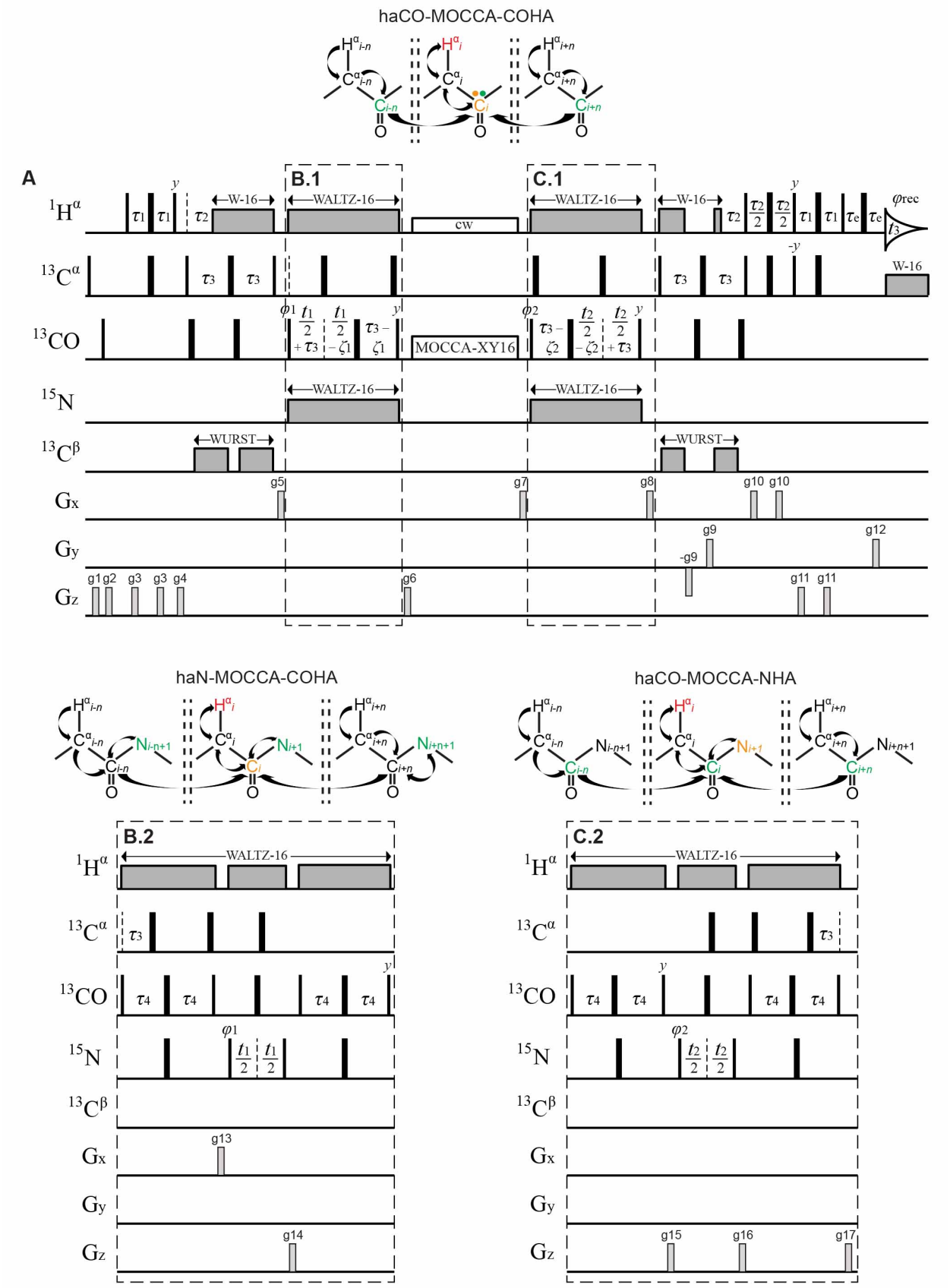
haCO-MOCCA-COHA
A
B.1
C.1
WALTZ-16
W-16
WURST
cw
MOCCA-XY16
haN-MOCCA-COHA
haCO-MOCCA-NHA
B.2
C.2

Figure S7. (A) Pulse sequence of the haCO-MOCCA-COHA experiment, providing correlations of the form (…,$^{13}CO_{i-1}$,$^{13}CO_i$,$^{13}CO_{i+1}$,…;$^{13}CO_i$;$^1H^{\alpha}_i$). Many of the experimental details are identical to those described in Figure 2 and are not repeated. ^1H, ^{13}C, and ^{15}N carriers are placed on water (~4.7 ppm), 58 ppm (until immediately before the ^{13}CO pulse of phase φ_1 when the carrier is jumped to 176 ppm and then returned to 58 ppm after the C.1 or C.2 elements are completed), and 119 ppm, respectively. A ^1H CW field of ~1.1 kHz is applied during the MOCCA scheme to continuously dephase water. The MOCCA-XY16 scheme[16,17] is made up of τ_{MC}–180°φ– τ_{MC} elements, where τ_{MC} = 4.32*pulse length of each ^{13}CO π pulse, adjusted in length to have a null for the $^{13}C^{\alpha}$ spins, and φ = 2(x,y), 2(y,x), 2(−x,−y), 2(−y,−x). Complete 16 step cycles are repeated l times to give the total mixing time (300 ms used here). The delays are: τ_1 = 1.8 ms, τ_2 = 3.6 ms (^{13}CH) or 2.3 ms (^{13}CH + $^{13}CH_2$), τ_3 = 4.5 ms, τ_4 = 15 ms, and τ_e accommodates the duration of gradient g12. ^{13}CO chemical shift evolution during t_1 and t_2 make use of semi-constant time schemes[14,15] as depicted in (B.1) and (C.1). The delay ζ_i is defined as ζ_i = {τ_3/(n_i-1)}x(ε-1), where n_i is the total number of complex points in the time domain and ε is set to the current complex t_i point number, ranging from 1 to n_i. Two other experiments, *i.e.* haN-MOCCA-COHA and haCO-MOCCA-NHA, can be performed by substituting (B.1) with (B.2), or (C.1) with (C.2), respectively. These two experiments involve additional magnetization transfers to ^{15}N for chemical shift encoding in t_1 and t_2, respectively so as to produce correlations of the form (…,$^{15}N_i$,$^{15}N_{i+1}$,$^{15}N_{i+2}$,…;$^{13}CO_i$;$^1H^{\alpha}_i$) (B.2) or (…,$^{13}CO_{i-1}$,$^{13}CO_i$,$^{13}CO_{i+}$,…;$^{15}N_{i+1}$;$^1H^{\alpha}_i$) (C.2). The phase cycle used for the two MOCCA-COHA experiments is: φ_1 = x,−x; φ_2 = 2(x),2(−x); and φ_{rec} = x,2(−x),x, while for the MOCCA-NHA scheme, φ_1 = 2(x),2(−x); φ_2 = x,−x; and φ_{rec} = x,2(−x),x. Quadrature detection in t_1 and t_2 is achieved by STATES-TPPI[10] of φ_1 and φ_2. Gradients are applied with the following durations (ms) and strengths (in % maximum): g1: (0.5, 24%), g2: (1.0, 24%), g3: (0.256, 15%), g4: (1.0, 40%), g5: (1.25, 80%), g6: (0.4, 25%), g7: (0.7, −50%), g8: (1.5, 80%), g9: (0.512, 90%), g10: (0.4, 40%), g11: (0.3, 15%), g12: (0.256, 90.3%), g13: (0.5, −40%), g14: (1.0, 15%), g15: (0.6, −50%), g16: (0.4, −30%), g17: (0.5, 20%). Magnetization transfer pathway of each experiment is depicted in separate cartoons, with chemical shift encoding color-coded as t_1 (green), t_2 (gold), and t_3 (red). In the cartoon for scheme (A) the chemical shift of the ^{13}CO that is labeled with both gold and green dots can be encoded during both t_1 and t_2 leading to a diagonal peak.

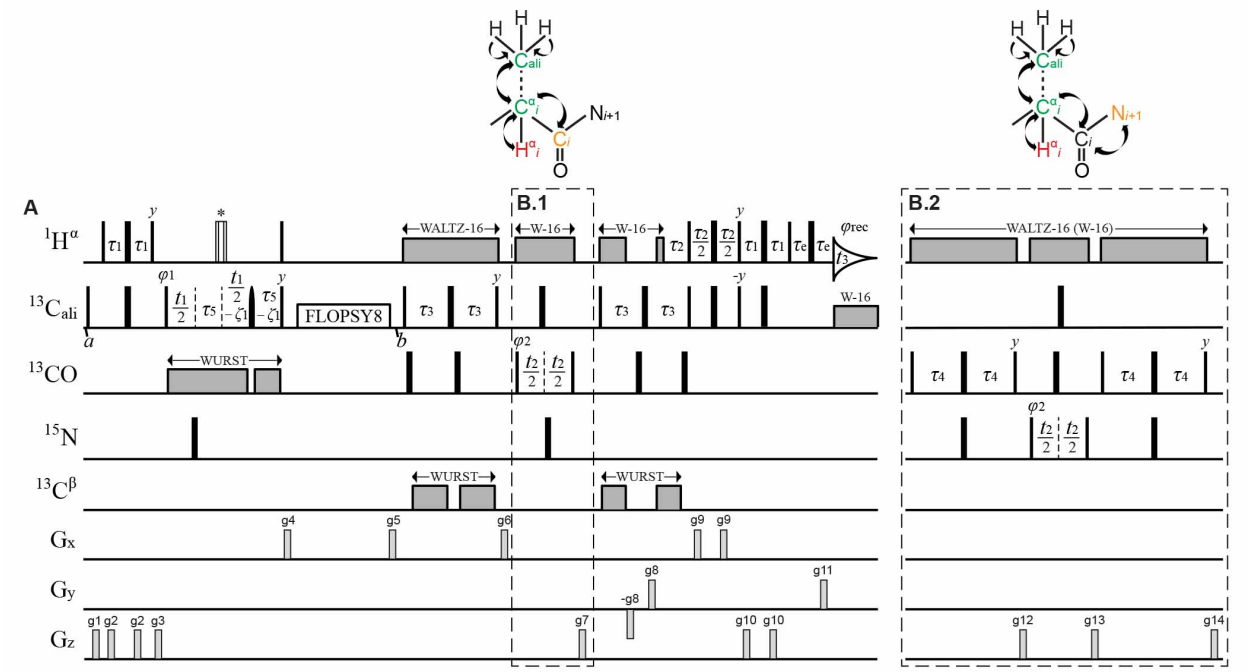

Figure S8. (A) Pulse sequence of the HCC-TOCSY-COHA experiment that generates correlations of the form ($^{13}C_i$,$^{13}CO_i$,$^{1}H^{\alpha}_i$), where $^{13}C_i$ are aliphatic carbons from the sidechain of residue i. Many of the details are described in the legend to Figure 2 and are not repeated. The ^{13}C carrier is initially positioned at 43 ppm (point *a*), shifted to 58 ppm at point *b*, to 176 ppm for the pulses in B.1 or B.2 and then back to 58 ppm. All ^{13}C rectangular pulses prior to the FLOPSY mixing period[18] are applied with the highest possible power, with a 400 µs REBURP pulse[13] during the t_1 interval to refocus aliphatic magnetization (centered at 43 ppm, 15.7 kHz B_1 field at maximum amplitude, 600 MHz). $^{13}C^{\alpha}$-^{13}CO couplings are suppressed during t_1 evolution through the application of ^{13}CO WURST decoupling (sweep of 14 ppm, centered at 176 ppm, 4 ms adiabatic pulses). The FLOPSY-8 mixing sequence is applied with a field of ~8.3 kHz for a total mixing time of 17 ms. Starting from point *b*, $^{13}C_{ali}$=$^{13}C^{\alpha}$ and ^{13}CO 90° and 180° rectangular pulses are applied with fields of $\Delta\Omega/\sqrt{15}$ and $\Delta\Omega/\sqrt{3}$, respectively, where $\Delta\Omega$ = 118 ppm[4]. The ^{1}H pulse denoted by an asterisk is of the composite variety[19], $90°_y$–$180°_x$–$90°_y$. The constant delays are: τ_1 = 1.8 ms, τ_2 = 3.6 ms (^{13}CH) or 2.3 ms (^{13}CH + $^{13}CH_2$), τ_3 = 4.5 ms, τ_4 = 15 ms, τ_5 = 1.15 ms, and τ_e is set to accommodate gradient g11. ^{13}C chemical shift evolution during t_1 makes use of semi-constant time schemes[14,15] where the delay ζ_1 is defined as $\zeta_1 = \{\tau_5/(n_1-1)\}x(\varepsilon-1)$, where n_1 is the total number of complex points in the time domain and ε is set to the current complex t_1 point number, ranging from 1 to n_1. ^{15}N chemical shift can be encoded in t_2 instead of ^{13}CO by substituting (B.1) with (B.2). The phase cycle is: $\varphi_1 = x,-x$; $\varphi_2 = 2(x),2(-x)$; and $\varphi_{rec} = x,2(-x),x$. Quadrature detection in t_1 and t_2 was achieved by STATES-TPPI[10] of φ_1 and φ_2, respectively. Gradients are applied with the following durations (ms) and strengths (in % maximum): g1: (0.5, 24%), g2: (0.256, 15%), g3: (1.0, 40%), g4: (0.7, −50%), g5: (0.7, −25%), g6: (0.8, 80%), g7: (0.4, 25%), g8: (0.512, 90%), g9: (0.4, 40%), g10: (0.3, 15%), g11: (0.256, 90.3%), g12: (0.6, −50%), g13: (0.4, −30%), g14: (0.5, 20%). Magnetization transfer pathways of both experiments are depicted in separate cartoons, where chemical shift encoding is color-coded as t_1 (green), t_2 (gold), and t_3 (red).

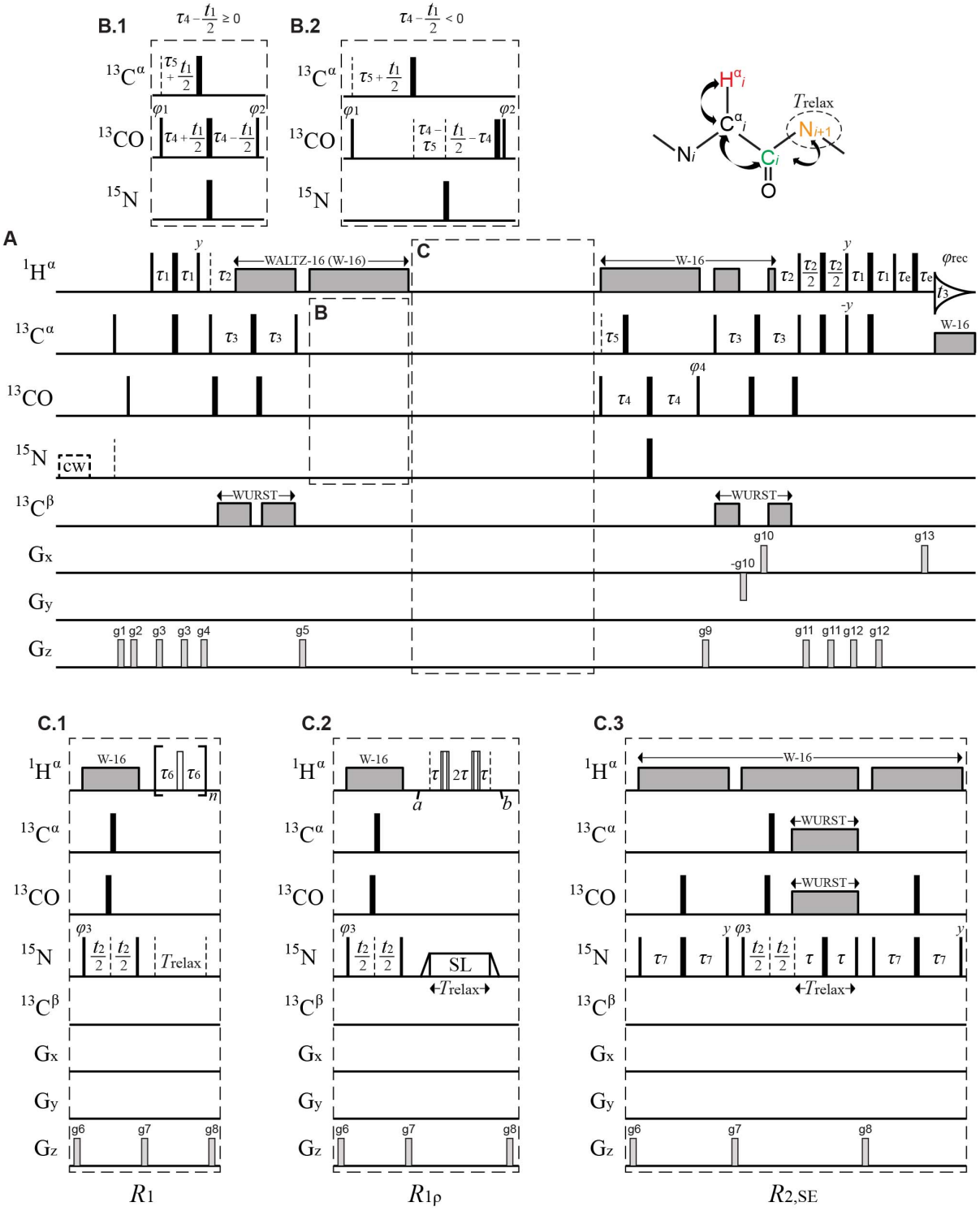

Figure S9. (A) Pulse sequences for measuring ^{15}N R_1, $R_{1\rho}$, and $R_{2,SE}$ relaxation rates based on the haCONHA scheme. The experiments can be performed as a collection of 3D or 2D datasets, with 2D versions used here. (B) ^{13}CO chemical shift evolution during t_1 is acquired in a semi-constant time

mode[14,15] as depicted in (B.1) and (B.2). (C) Sequences (C.1), (C.2), and (C.3) are used to measure R_1, $R_{1\rho}$, and $R_{2,SE}$, respectively. Many of the details are as in the legend to Figure 2 and are not repeated. The ^{13}C carrier is initially positioned at 58 ppm, shifted to 176 ppm at the start of block B and back to 58 ppm after the ^{13}CO 90° pulse of phase φ_4. In (C.1), a τ_6–180°$_x$– τ_6 element is repeated n times for the duration of T_{relax}, where ^1H 180° pulses are applied with a field that is 6 dB lower than maximum power, to suppress cross-correlation effects between ^1H-^{15}N dipolar and ^{15}N CSA relaxation mechanisms. In (C.2) a 2 kHz ^{15}N spin-lock field is employed for duration T_{relax}. Magnetization is 'placed' along the appropriate effective field using a 250 kHz adiabatically swept pulse of 4 ms duration, swept in the downfield direction, and swept upfield for the second pulse that positions the magnetization along the z axis. The ^1H carrier is shifted to the center of the amide region at point *a* and subsequently back to water at *b*. Two composite 90°$_y$–180°$_x$–90°$_y$ ^1H pulses are applied as indicated to suppress ^1H-^{15}N dipolar - ^{15}N CSA cross-correlations[20,21]. We have found it necessary to include an ^{15}N heat compensation element (dashed rectangle labeled CW at the start of the sequence) of duration $T_{relax,max} - T_{relax}$, where $T_{relax,max}$ is the maximum T_{relax} value used. This ensures that uniform heating is applied for all relaxation delays. (C.3) 'Pure' ^{15}N magnetization is generated prior to the spin-echo period by refocusing ^{15}N magnetization with respect to $^{13}C^{\alpha}$ and ^{13}CO. Subsequently, $^{13}C^{\alpha}$ and ^{13}CO WURST decoupling is achieved using a combined waveform that sweeps from 40 to 64 ppm (for $^{13}C^{\alpha}$) and from 169 to 183 ppm (for ^{13}CO). The delays are: τ_1 = 1.8 ms, τ_2 = 3.6 ms (^{13}CH) or 2.3 ms (^{13}CH + $^{13}CH_2$), τ_3 = 4.5 ms, τ_4 = 15 ms, τ_5 = 4.9 ms, τ_6 = 2.5 ms, τ_7 = 16.5 ms and τ_e accommodates gradient g13. The phase cycle is: $\varphi_1 = 2(x),2(-x)$; φ_2 =48.5° (600 MHz); $\varphi_3 = x,-x$; φ_4=48.5° (600 MHz); and $\varphi_{rec} = (x, -x, -x, x)$. Quadrature detection in t_1 and t_2 is achieved by STATES-TPPI[10] of φ_1 and φ_3, respectively. Gradients are applied with the following durations (ms) and strengths (in % maximum): g1: (0.5, 24%), g2: (1.0, 24%), g3: (0.256, 15%), g4: (1.0, 40%), g5: (1.25, 80%), g6: (1.5, 80%), g7: (0.9, 50%), g8: (0.9, 25%), g9: (1.0, 15%), g10: (0.512, 90%), g11: (0.4, 40%), g12: (0.3, 15%), g13: (0.256, 90.3%). The magnetization transfer pathway is depicted by the cartoon at the top, where chemical shift encoding is color-coded as t_1 (green), t_2 (gold), and t_3 (red).

As described in the text, the R_1 and $R_{1\rho}$ relaxation experiments measure the decay of two-spin elements of the form $^{15}N_j{}^{13}CO_z$ where j=z (R_1; ^{15}N magnetization along the z-axis) or z' ($R_{1\rho}$; ^{15}N magnetization locked along an effective axis that makes an angle θ with respect to the z-axis where θ = arctan($\nu_1/\Delta\Omega$), ν_1 is the spin-lock field strength and $\Delta\Omega$ is the offset of the spin in question from the carrier[22]; CO_z is the z-component of CO-magnetization). In principle, it is possible to first refocus anti-phase ^{15}N magnetization with respect to the attached ^{13}CO spin and subsequently record the relaxation of pure ^{15}N magnetization before reestablishing the two spin $^{15}N_x{}^{13}CO_z$ coherence en route to detection. Although advantageous in that the ^{13}CO T_1 would not enter into expressions for relaxation (unlike the case in Eqs 1-3 of the main text), the disadvantage is that a pair of additional delays must be inserted for refocusing anti-phase ($^{15}N_x{}^{13}CO_z \rightarrow {}^{15}N_x$) and defocusing in-phase ($^{15}N_x \rightarrow {}^{15}N_x{}^{13}CO_z$) ^{15}N magnetization. Our preference is, where possible, to maximize sensitivity as the anti-phase to in-phase to anti-phase cycle is associated with ~60 ms of additional transverse relaxation. The situation for recording the decay of ^{15}N magnetization via a simple spin-echo element (Figure panel C.3), that includes contributions from chemical exchange, is different. During the course of the T_{relax} period ^{15}N magnetization interconverts between in-phase ($^{15}N_x$) and anti-phase ($^{15}N_x{}^{13}CO_z$) components. (Note that in the $R_{1\rho}$ measurement this does not occur due to the 2 kHz ^{15}N spin lock). Consequently, the effective relaxation rate during T_{relax} will vary with τ as[20],

$$R_{2,eff} = 0.5(R_{2,A} + R_{2,I}) + \frac{1}{2}\frac{\sin(2\pi J_{NCO}\tau)}{2\pi J_{NCO}\tau}(R_{2,A} - R_{2,I}),\ 2\pi J_{NCO} \gg R_{2,A} - R_{2,I}$$

where $R_{2,A}$ and $R_{2,I}$ are the relaxation rates of $^{15}N_x{}^{13}CO_z$ and $^{15}N_x$, respectively, and 2τ is the duration of T_{relax}. This produces non-exponential decay curves, and, of course, erroneous relaxation rates. For values of $\tau = k/(2J_{NCO})$, k=0,1,2,…, $R_{2,eff} = 0.5(R_{2,A}+R_{2,I})$, but this limits the values of τ that can be chosen. We prefer, therefore, to ensure that ^{15}N transverse magnetization remains in-phase for the duration of the T_{relax} element, requiring the use of simultaneous $^{13}C^{\alpha}$ and ^{13}CO decoupling schemes during this period. Finally, although it is tempting to forgo the extra evolution periods associated with refocusing and defocusing ^{15}N magnetization and simply apply ^{13}CO decoupling to anti-phase magnetization ($^{15}N_x{}^{13}CO_z$) this would lead to erroneously short relaxation rates due to imperfections in decoupling.

Table S1

Experiment	t_{1max} (ms)	t_{2max} (ms)	t_{3max} (ms)	NS	Time (hr)	Remarks
Dilute CAPRIN1, 25 mM NaPi, pH 7.4, 30 °C; Comparison of S/N of $^{1}H^{\alpha}$- *vs* ^{13}C-detection						
haCONHA	64	55	64	2	21	τ_2 = 3.6 ms, gradient coherence transfer selection (GCTS)
..	..	..	..	8	21	τ_2 = 3.6 ms, GCTS, nus = 26 %
^{13}C-haCON	55	128		148	21	τ_2 = 3.6 ms; Acq data truncated to 64 ms prior to analysis – established that this did not affect S/N
haCONHA	64	55	64	2	3	τ_2 = 3.6 ms, GCTS, nus = 14 %
^{13}C-haCON	55	128		20	3	τ_2 = 3.6 ms; Acq data truncated to 64 ms prior to analysis
haCONHA	64	55	64	2	5	τ_2 = 2.3 ms, GCTS, nus = 25 %
^{13}C-haCON	55	128		36	5	τ_2 = 2.3 ms; Acq data truncated to 64 ms prior to analysis
Condensed CAPRIN1, 25 mM NaPi, pH 7.4, 100 mM NaCl, 40 °C; Comparison of S/N of $^{1}H^{\alpha}$- *vs* ^{13}C-detection						
haCONHA	64	55	64	2	21	τ_2 = 3.6 ms, GCTS
^{13}C-haCON	55	128		148	21	τ_2 = 3.6 ms; Acq data truncated to 64 ms prior to analysis
haCONHA	64	55	64	2	21	τ_2 = 2.3 ms, GCTS
^{13}C-haCON	55	128		148	21	τ_2 = 2.3 ms; Acq data truncated to 64 ms prior to analysis
Dilute CAPRIN1, 25 mM MES, pH 5.5, 25 °C; Comparison of S/N of $^{1}H^{\alpha}$- *vs* $^{1}H^{N}$-observe						
haCONHA	50	55	64	4	7	τ_2 = 2.3 ms, GCTS, nus = 16 %
HNCO	50	55	64	4	7	sensitivity-enhanced, water flip-back, nus = 16 %
Dilute CAPRIN1, 25 mM HEPES, pH 7.4, 25 °C; Comparison of S/N of $^{1}H^{\alpha}$- *vs* $^{1}H^{N}$-observe						
haCONHA	50	55	64	4	8	τ_2 = 2.3 ms, GCTS, nus = 25 %
HNCO	50	55	64	4	8	sensitivity-enhanced, water flip-back, nus = 25 %
Dilute CAPRIN1, 25 mM HEPES, pH 7.4, 30 °C; Assignment and Relaxation Studies						
haCONHA	50	55	64	4	8	τ_2 = 2.3 ms, GCTS, nus = 25 %

haNCOHA	55	50	64	4	8	τ_2 = 2.3 ms, GCTS, nus = 25 %
haCO-MOCCA-COHA	50	50	64	2	6	τ_2 = 2.3 ms, GCTS, nus = 30 %, d_1 = 2 s, mixing = 300 ms
haN-MOCCA-COHA	55	50	64	2	10	τ_2 = 2.3 ms, GCTS, nus = 30 %, d_1 = 2 s, mixing = 300 ms
haCO-MOCCA-NHA	53	55	64	2	11	τ_2 = 2.3 ms, GCTS, nus = 30 %, d_1 = 2 s, mixing = 300 ms
HCC-TOCSY-COHA	7	53	64	4	5	τ_2 = 2.3 ms, GCTS, nus = 30 %, d_1 = 1 s, mixing = 17 ms
$R_{1\rho}$	0	49	64	12	11	τ_2 = 2.3 ms, GCTS, d_1 = 2 s, T_{relax} = {5, 50, 100, 150, 200, 248}
R_1	0	49	64	12	4	τ_2 = 2.3 ms, GCTS, d_1 = 1 s, T_{relax} = {10, 50, 125, 250 ms}
$R_{2,SE}$	0	49	64	12	4	τ_2 = 2.3 ms, GCTS, d_1 = 1 s, T_{relax} = {0, 50, 100, 150, 200 ms}
Dilute CAPRIN1, 25 mM HEPES, pH 7.4, 2.5 mM PPi, 30 °C; Assignment and Relaxation Studies						
haCONHA	50	55	64	4	8	τ_2 = 2.3 ms, GCTS, nus = 25 %
HCC-TOCSY-COHA	7.5	53	64	4	11	τ_2 = 2.3 ms, GCTS, nus = 50 %, d_1 = 1 s, mixing = 17 ms
$R_{1\rho}$	0	49	64	12	11	τ_2 = 2.3 ms, GCTS, d_1 = 2 s, T_{relax} = {5, 50, 100, 150, 200, 248 ms}
R_1	0	49	64	12	4	τ_2 = 2.3 ms, GCTS, d_1 = 1 s, T_{relax} = {10, 50, 125, 250, 50 ms}
$R_{2,SE}$	0	49	64	12	4	τ_2 = 2.3 ms, GCTS, d_1 = 1 s, T_{relax} = {0, 50, 100, 150, 200 ms}

References

(1) Kay, L. E.; Xu, G. Y.; Yamazaki, T. Enhanced-Sensitivity Triple-Resonance Spectroscopy with Minimal H2O Saturation. *J. Magn. Reson. Ser. A* **1994**, *109* (1), 129–133. https://doi.org/10.1006/jmra.1994.1145.

(2) Yuwen, T.; Skrynnikov, N. R. CP-HISQC: A Better Version of HSQC Experiment for Intrinsically Disordered Proteins under Physiological Conditions. *J. Biomol. NMR* **2014**, *58* (3), 175–192. https://doi.org/10.1007/s10858-014-9815-5.

(3) Shaka, A. J.; Keeler, J.; Frenkiel, T.; Freeman, R. An Improved Sequence for Broadband Decoupling: WALTZ-16. *J. Magn. Reson.* **1983**, *52* (2), 335–338. https://doi.org/10.1016/0022-2364(83)90207-X.

(4) Kay, L. E.; Ikura, M.; Tschudin, R.; Bax, A. Three-Dimensional Triple-Resonance NMR Spectroscopy of Isotopically Enriched Proteins. *J. Magn. Reson.* **1990**, *89* (3), 496–514. https://doi.org/10.1016/0022-2364(90)90333-5.

(5) Vuister, G. W.; Bax, A. Resolution Enhancement and Spectral Editing of Uniformly 13C-Enriched Proteins by Homonuclear Broadband 13C Decoupling. *J. Magn. Reson.* **1992**, *98* (2), 428–435. https://doi.org/10.1016/0022-2364(92)90144-V.

(6) Kupče, Ē.; Freeman, R. Adiabatic Pulses for Wideband Inversion and Broadband Decoupling. *J. Magn. Reson. Ser. A* **1995**, *115* (2), 273–276. https://doi.org/10.1006/jmra.1995.1179.

(7) Kupče, E.; Wagner, G. Multisite Band-Selective Decoupling in Proteins. *J. Magn. Reson. - Ser. B* **1996**, *110* (3), 309–312. https://doi.org/10.1006/jmrb.1996.0048.

(8) Yang, D.; Nagayama, K. A Sensitivity-Enhanced Method for Measuring Heteronuclear Long-Rangé Coupling Constants from the Displacement of Signals in Two 1D Subspectra. *J. Magn. Reson. - Ser. A* **1996**, *118* (1), 117–121. https://doi.org/10.1006/jmra.1996.0017.

(9) Ottiger, M.; Delaglio, F.; Bax, A. Measurement of J and Dipolar Couplings from Simplified Two-Dimensional NMR Spectra. *J. Magn. Reson.* **1998**, *131* (2), 373–378. https://doi.org/10.1006/jmre.1998.1361.

(10) Marion, D.; Ikura, M.; Tschudin, R.; Bax, A. Rapid Recording of 2D NMR Spectra without Phase Cycling. Application to the Study of Hydrogen Exchange in Proteins. *J. Magn. Reson.* **1989**, *85* (2), 393–399. https://doi.org/10.1016/0022-2364(89)90152-2.

(11) Kay, L. E.; Keifer, P.; Saarinen, T. Pure Absorption Gradient Enhanced Heteronuclear Single Quantum Correlation Spectroscopy with Improved Sensitivity. *J. Am. Chem. Soc.* **1992**, *114* (26), 10663–10665. https://doi.org/10.1021/ja00052a088.

(12) Schleucher, J.; Sattler, M.; Griesinger, C. Coherence Selection by Gradients without Signal Attenuation: Application to the Three□Dimensional HNCO Experiment. *Angew. Chemie Int. Ed. English* **1993**, *32* (10), 1489–1491. https://doi.org/10.1002/anie.199314891.

(13) Geen, H.; Freeman, R. Band-Selective Radiofrequency Pulses. *J. Magn. Reson.* **1991**, *93* (1), 93–141. https://doi.org/10.1016/0022-2364(91)90034-Q.

(14) Grzesiek, S.; Anglister, J.; Bax, A. Correlation of Backbone Amide and Aliphatic Side-Chain Resonances in 13C/15N-Enriched Proteins by Isotropic Mixing of 13C Magnetization. *J. Magn. Reson. Ser. B* **1993**, *101* (1), 114–119. https://doi.org/10.1006/jmrb.1993.1019.

(15) Logan, T. M.; Olejniczak, E. T.; Xu, R. X.; Fesik, S. W. A General Method for Assigning NMR

Spectra of Denatured Proteins Using 3D HC(CO)NH-TOCSY Triple Resonance Experiments. *J. Biomol. NMR* **1993**, *3* (2), 225–231. https://doi.org/10.1007/BF00178264.

(16) Furrer, J.; Kramer, F.; Marino, J. P.; Glaser, S. J.; Luy, B. Homonuclear Hartmann-Hahn Transfer with Reduced Relaxation Losses by Use of the MOCCA-XY16 Multiple Pulse Sequence. *J. Magn. Reson.* **2004**, *166* (1), 39–46. https://doi.org/10.1016/j.jmr.2003.09.013.

(17) Yoshimura, Y.; Kulminskaya, N. V.; Mulder, F. A. A. Easy and Unambiguous Sequential Assignments of Intrinsically Disordered Proteins by Correlating the Backbone 15N or 13C' Chemical Shifts of Multiple Contiguous Residues in Highly Resolved 3D Spectra. *J. Biomol. NMR* **2015**, *61* (2), 109–121. https://doi.org/10.1007/s10858-014-9890-7.

(18) Kadkhodaie, M.; Rivas, O.; Tan, M.; Mohebbi, A.; Shaka, A. J. Broadband Homonuclear Cross Polarization Using Flip-Flop Spectroscopy. *J. Magn. Reson.* **1991**, *91* (2), 437–443. https://doi.org/10.1016/0022-2364(91)90210-K.

(19) Leviti, M. H.; Freeman, R. NMR Population Inversion Using a Composite Pulse. *J. Magn. Reson.* **1979**, *33* (2), 473–476. https://doi.org/10.1016/0022-2364(79)90265-8.

(20) Palmer, A. G.; Skelton, N. J.; Chazin, W. J.; Wright, P. E.; Rance, M. Suppression of the Effects of Cross-Correlation between Dipolar and Anisotropic Chemical Shift Relaxation Mechanisms in the Measurement of Spin-Spin Relaxation Rates. *Mol. Phys.* **1992**, *75* (3), 699–711. https://doi.org/10.1080/00268979200100511.

(21) Kay, L. E.; Nicholson, L. K.; Delaglio, F.; Bax, A.; Torchia, D. A. Pulse Sequences for Removal of the Effects of Cross Correlation between Dipolar and Chemical-Shift Anisotropy Relaxation Mechanisms on the Measurement of Heteronuclear T1 and T2 Values in Proteins. *J. Magn. Reson.* **1992**, *97* (2), 359–375. https://doi.org/10.1016/0022-2364(92)90320-7.

(22) Palmer, A. G.; Kroenke, C. D.; Loria, J. P. Nuclear Magnetic Resonance Methods for Quantifying Microsecond-to-Millisecond Motions in Biological Macromolecules. In *Methods in Enzymology*; 2001; Vol. 339, pp 204–238. https://doi.org/10.1016/S0076-6879(01)39315-1.